Ultra-dense nodal seismic acquisition for automated geohazard analysis

Daniele Colombo[1], Ernesto Sandoval-Curiel[1], Taqi Alyousuf[1], Ersan Turkoglu[1], and Diego Rovetta[2]

https://doi.org/10.1190/tle43080484.1

Abstract

In this paper, we address the problem of shallow geohazard mapping by developing an integrated workflow consisting of nodal seismic acquisition and automated data analysis. Densely spaced point-receiver land nodes and point sources are adopted as an alternative to receiver arrays or groups conventionally used in seismic exploration. The recently developed methodology of surface-consistent decomposition of the transmitted wavefield is applied to the nodal data. Ultra-resolution mapping of surface-consistent attributes in amplitude and phase is obtained, together with the generation of high-energy signal beams at the common midpoint positions, forming virtual (shot) supergathers (VSGs). The VSG preserves frequency and true-amplitude content thanks to the surface-consistent corrections applied before beam forming. Traveltimes, waveforms, and surface waves are then analyzed in the high signal-to-noise ratio VSG, leading to inversion of the subsurface parameters. Human-intensive interpretation of surface-wave dispersion curves in the *f-k* spectra is facilitated by the introduction of efficient machine learning algorithms for the unsupervised and supervised paradigms. The ultra-dense nodal acquisition and automated data analysis are effectively applied to the analysis of several cases of near-surface geohazards.

Introduction

Fast and reliable identification and imaging of geohazards in the shallow subsurface is becoming a stringent requirement in sustainability objectives such as safe installation of wind turbines, subsidence due to permafrost thawing, installation of monitoring devices for carbon capture and sequestration (CCS), and business continuity in drilling. Shallow geohazards are often found in areas where near-surface formations, such as carbonates and evaporites, are subject to dissolution due to the circulation of water. Karst landscapes can develop with exposed sinkholes and subterranean rivers that flow in a network of connected caves. In other cases, sinkholes and fracture-related cavities are covered by sediments (e.g., compacted aeolian sands) and are not visible from the surface. The buried cavities or mechanically weakened rock formations pose a threat to humans and infrastructure because catastrophic collapses can occur due to increase in load, construction activities, or increase in pore pressure caused by fluids (e.g., heavy rain or pressurized drilling fluids). High-resolution shallow geophysical investigation is typically conducted to characterize the near surface. Commonly used techniques include direct-current resistivity (e.g., electric resistivity tomography), analysis of surface waves (e.g., multichannel analysis of surface waves [MASW]), microgravity, low-frequency ground-penetrating radar, and transient electromagnetics. Most approaches, including gravity, electric and diffusion-based electromagnetic methods, are high resolution for the near surface. Effectiveness of the different techniques is related to the nature of the subsurface anomaly (i.e., geophysical properties) and to the characteristics and lithology of the rock substratum. Standard shallow geophysical techniques are typically 2D and suffer from the presence of surface obstacles when running cables. The human-intensive data analysis involved makes the standard approaches suited for limited-size surveys. Extensive applications of high-resolution shallow geohazard investigation require a rethink of the acquisition and data analysis techniques, with the objectives of boosting resolution, automating data analysis, and providing fast turnaround time for effective decision making. Such objectives involve all aspects of the geophysical value chain including acquisition, automated processing, and fast and robust data interpretation.

High-resolution seismic surveys provide one of the best opportunities for investigating shallow geohazards, especially when all components of the elastic wave propagation are considered in the analysis. The drawback of dense 3D seismic acquisitions is related to complex operations with bulky equipment, as well as to lengthy and costly data analysis and inversion processing. This discourages 3D seismic acquisition from becoming a practical tool for fast-turnaround shallow geohazard analysis. However, new opportunities have surfaced in point-source/point-receiver acquisitions, which are now enabled by efficient and low-cost standalone nodal technology that utilizes wireless communication. Nodal seismic acquisition has found immediate application in the marine environment, where signal-to-noise ratio (S/N) and near-surface complexities are of lesser concern. However, point-receiver land seismic applications (Dean et al., 2018) are more difficult because the near surface poses a challenge for low S/N and kinematic and dynamic signal distortions introduced by the weathering layer. Discussions on whether data should be acquired through single sensors or arrays have occupied geophysicists over the last couple of decades, and the topic is still debated (Ourabah, 2024). In the image domain, the use of point-receiver or array data should not matter. The problem arises because achieving the imaging step necessitates several preliminary operations to be performed on low S/N gathers, such as the derivation of operators for data processing and the building of reliable velocity models (e.g., time-domain velocity analysis or full-waveform inversion [FWI]). Such S/N problems can be addressed by digital group forming in the prestack domain if appropriate near-surface corrections and data preconditioning can be applied early in the processing sequence. The amount of data involved in nodal acquisitions also points to the necessity of

Manuscript received 14 March 2024; revision received 11 May 2024; accepted 29 May 2024.

[1]Saudi Aramco, EXPEC Advanced Research Center, Dhahran, Saudi Arabia. E-mail: daniele.colombodc@outlook.com; ernesto.sandovalcuriel@aramco.com; taqi.yousuf@aramco.com; ersan.turkoglu@aramco.com.
[2]Aramco Overseas, Delft Research Center, Delft, Netherlands. E-mail: diego.rovetta.1@aramcooverseas.com.

synthesizing, in statistical terms, the densely sampled signal (e.g., through the generation of high S/N beams that would facilitate the operations of inversion and imaging).

To target these objectives, we began the development of a novel suite of tools focused on statistical data analysis (Colombo et al., 2016) with machine learning (ML) support (Alyousuf et al., 2018; Colombo et al., 2021b, 2024; Rovetta et al., 2021), collectively termed "intelligent near-surface platform." The signal processing and inversion tools are designed to boost the subsurface imaging resolution while utilizing a fraction of the time requested by standard approaches. The underlying assumption is represented by a dense continuous sampling of the subsurface and of the propagated seismic wavefield to enable a statistical and ML approach to data-driven preconditioning and inversion. Such characteristics are provided by point-receiver nodal acquisitions. In this paper, we detail a fast and accurate scheme for shallow geohazard analysis that relies on ultra-dense acquisition of point-source/point-receiver seismic data using wireless nodes. The resulting densely sampled wavefield is statistically analyzed by deriving near-surface velocities and corrections in phase and amplitude, based on surface-consistent decomposition of the transmitted wavefield. High S/N group and beam forming are then implemented for the automatic analysis of multiple seismic phases, including surface waves, as well as the transmitted and reflected wavefields. ML-based developments are applied to automate human-intensive tasks (e.g., surface-wave dispersion curve picking) and to enhance inversion through physics-driven deep learning approaches. The resulting intelligent near-surface workflow is applied to the analysis of shallow geohazards.

Acquisition

The developed seismic workflow for geohazard analysis relies on a dense sampling of the propagated seismic wavefield, as obtained from narrow-spaced nodes and shotpoints (SPs). A carpet layout is adopted where the whole area of interest is occupied by equally spaced nodes and interleaved and staggered SP positions. Each receiver of the mesh is active for 24 hours during the acquisition so the active source signal and passive noise recordings are obtained for the same survey. SP configurations follow a similar pattern with similar spacing. Acquisition layouts of this type have been tested to date with a node spacing of 5 × 5 m and SP spacing up to 2.5 × 5 m (Figure 1). The carpet acquisition layout is more efficient when compared to a roll-along configuration using fewer nodes.

This translates to less fieldwork with a simplified layout, enabling fast node deployment in 2–3 days, followed by 10 days of production shot acquisition for the case illustrated in Figure 1. The data generated include 91 million traces, obtained from 7381 SP locations with three repetitions vertically stacked, and 4094 receiver nodes. The recorded seismic data set (Figure 1) amounts to approximately 1 TB of data, with time sampling of 2 ms and clock accuracy in the range of 100 μs at the time of synchronization with the duty-cycled GPS. The full acquisition and data retrieval were accomplished in two weeks. The utilized source includes an autofire accelerated impact energy source with a nitrogen-powered spring capable of generating high S/N records to the longest source-receiver offset (Figure 1b). Two types of vertical-component seismic nodes were utilized in different surveys. Nodes equipped with piezoelectric accelerometer sensors and a frequency response of 1–125 Hz (Ourabah, 2024) were employed in the case shown in Figure 1. Geophone-based nodes with a natural frequency of 5 Hz (Zeckra et al., 2022) were utilized in the other applications. The flexibility provided by the nodal acquisition system enables us to overcome previously experienced difficulties related to fences and pipelines. Microgravity complements nodal seismic acquisition in all of the investigated areas and provides an important verification tool. Microgravity spatial sampling is 5 × 5 m, consistent with the seismic nodes. Gravity acquisition specifications are tuned to ensure a 5 μGal repetition error (first standard deviation). Gravity processing follows a standard scheme that involves free air and Bouguer corrections, as well as terrain corrections where a detailed digital elevation model, obtained from the dedicated topographic survey, is adopted.

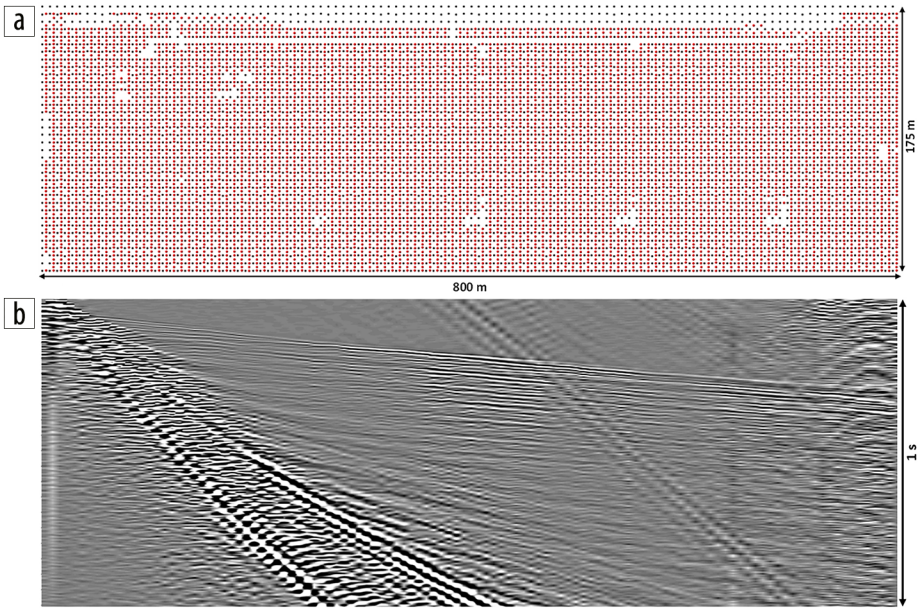

Figure 1. (a) Nodal seismic carpet acquisition (red circles are seismic sources; black circles are seismic nodes), where the gaps in source sampling in the southern section are related to fences. (b) Test shot acquired along the southern edge of the investigated area.

Data analysis method

The dense spatial sampling of the seismic wavefield introduces the possibility of statistical analysis of the seismic data in the spatial/temporal domains. The objective is to determine surface-related kinematic and dynamic distortions (possibly frequency dependent), correct the propagated wavefield, form groups and beam the data for enhanced S/N, and invert for the subsurface properties. Statistics are embedded in every step, and ML is utilized to

streamline certain human-intensive operations. The suite of tools forms an evolving intelligent near-surface analysis package that is robust and provides the necessary analysis for shallow geohazard detection and imaging. The key components of the approach are summarized next.

Diving-wave surface-consistent decomposition. Deriving surface-consistent corrections in phase and amplitude from reflected waves is a lengthy process that requires heavy data processing, denoising, and repeated velocity analysis. These become difficult to perform for shallow seismic data due to the effects of noise and presence of large-amplitude surface waves. To streamline this step, we opt for the surface-consistent decomposition of the transmitted wavefield (e.g., diving waves), for which the S/N is typically high on raw gathers. The convolutional model of the wave propagation is recast in terms of the transmitted wavefield, as described by Colombo et al. (2016, 2020, 2021a). Seismic traces are collected in a dedicated sorting domain, encompassing midpoint (e.g., X-Y) and source-receiver offset (e.g., O), to generate a hypercube in XYO sorting (where azimuth A can optionally be added to the sorting scheme XYOA). The traces collected in the XYO domain are used to generate a pilot trace by stacking, after performing some automated residual moveout corrections and noisy trace elimination. Individual trace phase and amplitude residuals are evaluated relative to the pilot trace and inverted for the source and receiver positions (surface-consistent analysis). The operation generates phase and amplitude corrections (optionally as a function of frequency) that are used to correct the individual traces for the near-surface distortions. These are performed by means of scalar time corrections of the phase. This corresponds to a linear phase correction in the frequency domain for the average phase distortion (Taner et al., 1974; Taner and Koehler, 1981). Amplitude distortions can be evaluated as scalars or by the derivation of a frequency-dependent operator when data exhibit viscoelastic behavior. In the latter case, the correction is performed by deconvolving the derived operator through spectral ratios (near-surface deconvolution) (Colombo et al., 2020). Finally, the spatial representation of surface-consistent time phase residuals, as well as of the amplitude residuals, provides informative attributes of the near surface that are used for diagnostic analysis of the ultra-shallow geologic conditions.

Group and beam forming: Virtual supergather. Surface-consistent decomposition of the transmitted wavefield and the associated corrections return traces that have been modified by removing near-surface distortions. Notice that no signal processing/conditioning is performed at this stage, and the seismic data fully preserve the frequency content and dynamic character with only surface-consistent corrections applied. Seismic traces are now suited for operations of group and beam forming for S/N enhancement. Various options may be available at this point. Traces may be stacked locally to digitally form a group, representing a beam of seismic signals, or nearby shot gathers may be grouped to form supergathers. The possible limitation of these approaches is that multiple subsurface midpoints may represent different geologic conditions.

In our implementation, we opt for group and beam forming in the XYO domain, where the pilot traces obtained from the previous step are collected for each midpoint and for all the offset bins to form a (shot) virtual supergather (VSG). Here, we must observe that the group and beam forming operations can be performed also in the azimuthal domain by the definition of an additional azimuthal bin (i.e., XYOA domain). The XYOA domain preserves the 3D information during beam forming. In most applications, and for shallow geohazard investigations, we found that the XYO-VSG domain (essentially 1.5D) is adequate and provides S/N enhancement while preserving amplitude fidelity and frequency content thanks to the surface-consistent corrections applied before summation. The VSG represents a midpoint-based volumetric seismic beam, showing the characteristics of a prestack shot gather of largely enhanced signal. The VSG domain becomes particularly useful for effectively decimating large seismic data sets while preserving frequency and dynamic characteristics (Figures 2a and 2b). The VSGs are then used for enhancing and scaling down several intensive operations of seismic data processing (e.g., FB picking, surface-wave phase velocity analysis, reflection velocity picking, and 1.5D FWI) (Colombo et al., 2021a).

Surface-wave analysis via ML. Rayleigh waves are recorded from conventional impulsive seismic sources emitting primarily compressive (P) waves. The analysis of surface waves (e.g., through the dispersion curve phase velocity inversion) has shown great potential for detecting and imaging shallow geohazards. The well-known technique of MASW (Park et al., 1999) is universally applied for geotechnical applications. The standard approach consists of 2D seismic profiling with a limited number of channels (e.g., 24, 48, 96) and an impact source (e.g., sledgehammer, accelerated weight drop, etc.). Related processing consists of a 2D Fourier transform (*f-k* domain) mapping the dispersive wavefield into phase velocity versus frequency spectra, where propagation modes are identified and picked for the successive inversion step. Surface waves (Rayleigh) are primarily sensing the shear (S) velocity because their particle motion provides limited sensitivity to the compressional P component. Sensitivity to V_P increases for modes beyond the fundamental mode. Higher modes, however, may be more difficult to recognize consistently

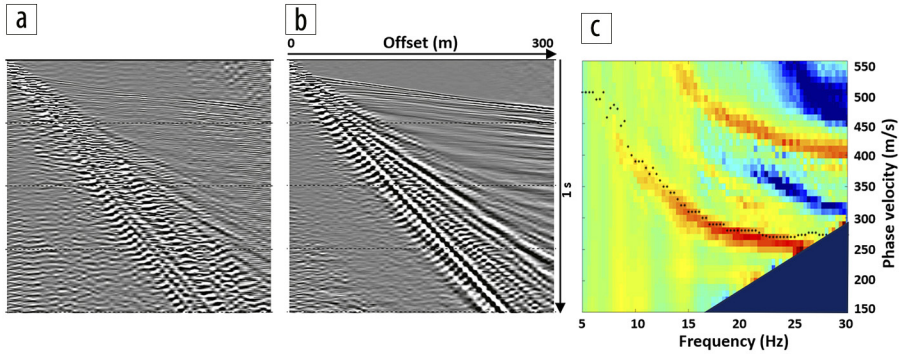

Figure 2. Comparison of: (a) single-fold shot gather, (b) corresponding VSG beam, and (c) VSG spectrum of phase velocity versus (c) frequency. Picking of the dispersion curve fundamental mode (dots) is performed via the unsupervised DBSCAN approach.

through gathers because they may not always be present or detectable. The primary application of surface waves is related to picking the fundamental propagation mode in the phase velocity/frequency spectrum and the successive inversion for the V_S model, where Poisson's ratio and density are provided as constants for a certain area. The phase velocity versus frequency analysis provides a broad sensitivity to shallow geologic features, and the inversion generates high-resolution near-surface V_S models (e.g., typically up to 30 to 50 m depth, depending on the frequency content). Bottlenecks in the broad utilization of surface waves for velocity modeling are related to the operation of picking the dispersion curves (e.g., fundamental mode). For this purpose, beam forming of dense wavefield sampling with VSG generation provides several benefits, such as useful data decimation, S/N enhancement, and more objective volumetric evaluation of the average surface wave dispersion around each subsurface position (Figure 2c). The S/N is enhanced to the point that ML approaches can be effectively implemented for automating the picking of dispersion curves (i.e., a tedious and time-consuming task).

We developed two ML schemes for dispersion curve picking based on unsupervised and supervised approaches. The first approach consists of an unsupervised method (Rovetta et al., 2021), where we adopt the density-based spatial clustering of applications with noise (DBSCAN) algorithm (Ester et al., 1996), which is suited for clusters of arbitrary shape. The windowed spectral energy is picked for the maximum value for each frequency and VSG. This generates a cloud of 3D points with dimensions of phase velocity, frequency, and VSG number. The DBSCAN algorithm is then applied to the points to identify clusters as 3D surfaces corresponding to different propagation modes. The method is highly efficient and robust to noise and requires the definition of only one input parameter, automatically derived, with the definition of a suitable search window. A benefit of ultra-dense spatial wavefield sampling and beam forming is that the algorithm allows clustering along a surface, where the extent is set by a user-defined search radius. The second method is based on a supervised ML scheme through neural networks based on field data training on a distributed number of samples and application of the trained network to the full field data set (Alyousuf et al., 2018). The approach is also very efficient, and the dispersion curve picking for several thousand shots is performed in a few hours, including the neural network training. Also, in this case, the downsampling and beam forming through VSG generation provide advantages in terms of enhanced S/N and 3D wavefield sampling. The two schemes (unsupervised and supervised) can further be joined through dedicated workflows. Inversion for a 1D V_S model is performed by means of forward modeling (Xia et al., 2003; Socco et al., 2009; Socco et al., 2010; Roy et al., 2013; Li and Hanafy, 2016; Miao et al., 2016) and preconditioned conjugate gradients. Figure 2c shows an example of the application of the unsupervised DBSCAN method to automatic picking of dispersion curves for the nodal acquisition for shallow geohazards shown in Figure 1.

Field applications

Different field applications were performed with nodal seismic technology by applying the described processing workflow.

Pilot areas — Preventive approach. Several nodal acquisitions and subsequent processing were performed for candidate areas to evaluate the potential of geohazards. The goal is to perform fast and reliable screening of the candidate locations.

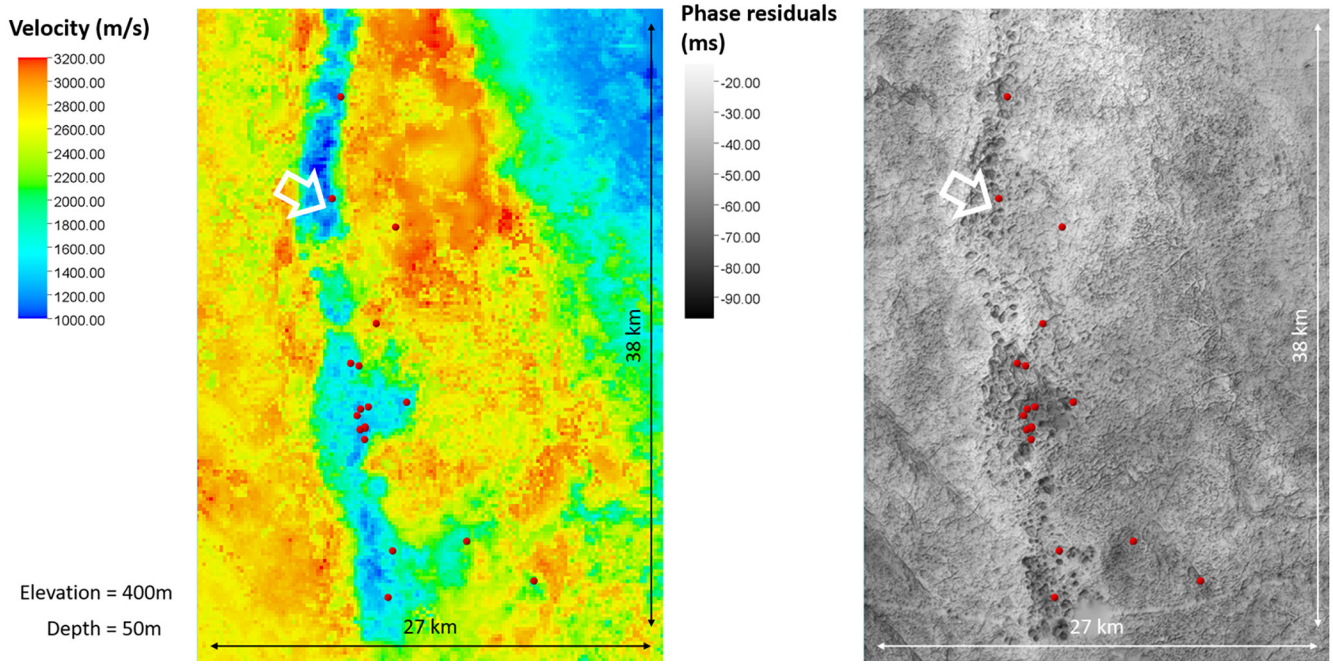

Figure 3. Pilot area 1 was investigated for geohazards by using the developed workflow applied to seismic exploration data. A low P-velocity corridor (left), as well as in an area displaying surface-consistent residual statics anomalies resembling circular features or karsts (right), is evidenced by the analysis. Red dots indicate the experienced sinkhole locations. The proposed site (arrows) is in the hazard area, and it is further investigated with high-resolution nodal seismic and microgravity.

DOI:10.1190/tle43080484.1

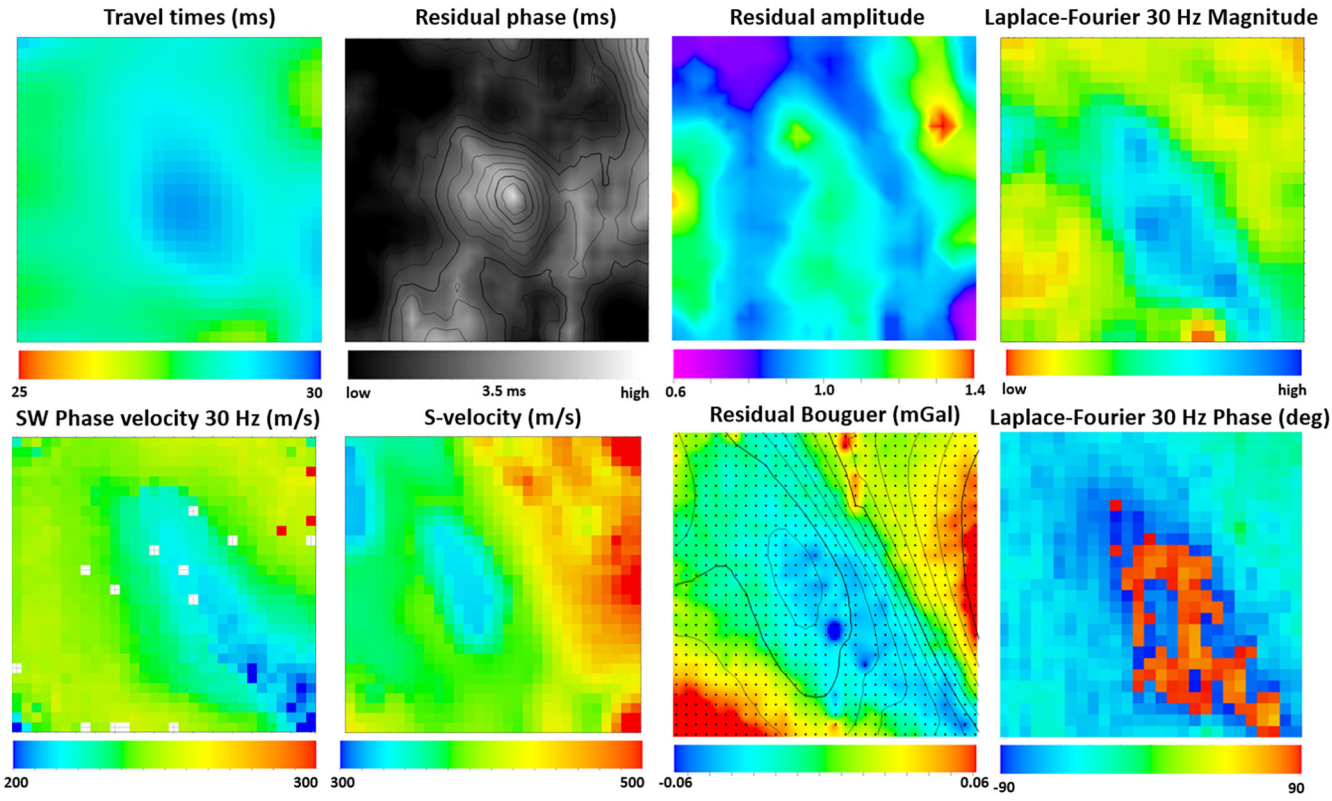

Figure 4. Pilot area 1. Combined geophysical attribute maps where the investigated area is 150 × 150 m with 5 × 5 m source and receiver spacing. The isolines in the residual Bouguer map indicate the topographic relief, and the dots represent the gravity station locations coincident with the seismic node locations.

Pilot area 1 is in a broader context that was previously investigated for shallow geohazards by using the surface-consistent workflow described and applied to seismic exploration data. The results of the analysis indicate a low-velocity corridor characterized by surface-consistent phase anomalies or residual statics resembling circular features (Figure 3). The striking relationship between the map of velocity and residual statics with the geologic evidence of karsts supports the correlation of geohazards with the shallow geologic conditions. Regional zonation of the shallow hazards can be performed through analysis of the near-surface geology and shallow geophysical properties. For the specific area, an initial assessment of the near-surface conditions can be based on the occurrence of selected locations in the low-velocity corridor/large residual phase features. The proposed site (arrows in Figure 3) is in the anomalous area. As such, it was investigated using the high-resolution acquisition/analysis workflow. The combined geophysical attribute maps (Figure 4) indicate the presence of a slightly elongated anomaly that develops from the center of the area toward the southeast corner. The anomaly seems to be correlated to the topographic low, but it is not completely collocated, as it develops more to the southeast. A depression at a very shallow depth may be indicative of weak rock formations such as a filled sinkhole. A cross section of V_S through the investigated area (Figure 5) indicates the presence of a shallow depression slightly shifted toward the east relative to the topographic depression. Based on the results, the site was ranked as unsafe.

Pilot area 2 contains a previously developed platform, as evidenced by the accurate topographic survey (Figure 6). The

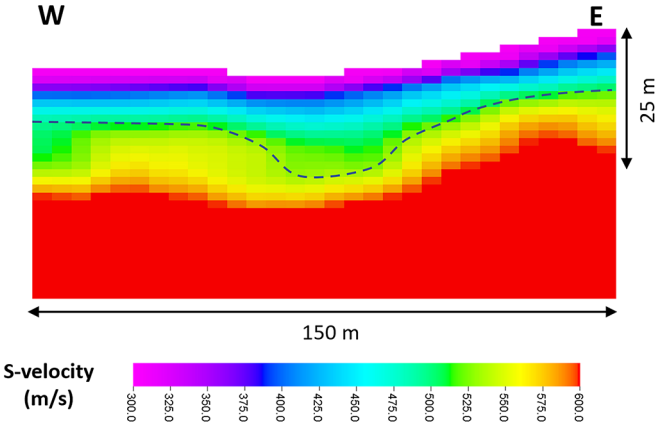

Figure 5. Pilot area 1. Cross section of V_S through the investigated area, indicating the presence of a shallow depression.

application of the geophysical workflow provides a suite of geophysical attributes, where we can distinguish between a very shallow response (top row in Figure 6) and a slightly deeper response (bottom row in Figure 6). In particular, we can observe how the dense nodal acquisition setup and automatic data analysis of the point-source/point-receiver nodal seismic data provide the high-resolution imaging of the central platform from the point of view of a surface-consistent residual amplitude, the high-frequency surface-wave phase velocity at 35 Hz, and the corresponding V_S inversion from surface to a depth of 4 m. Slightly deeper (e.g., 10 m depth and below; Figure 6 bottom row), the geophysical

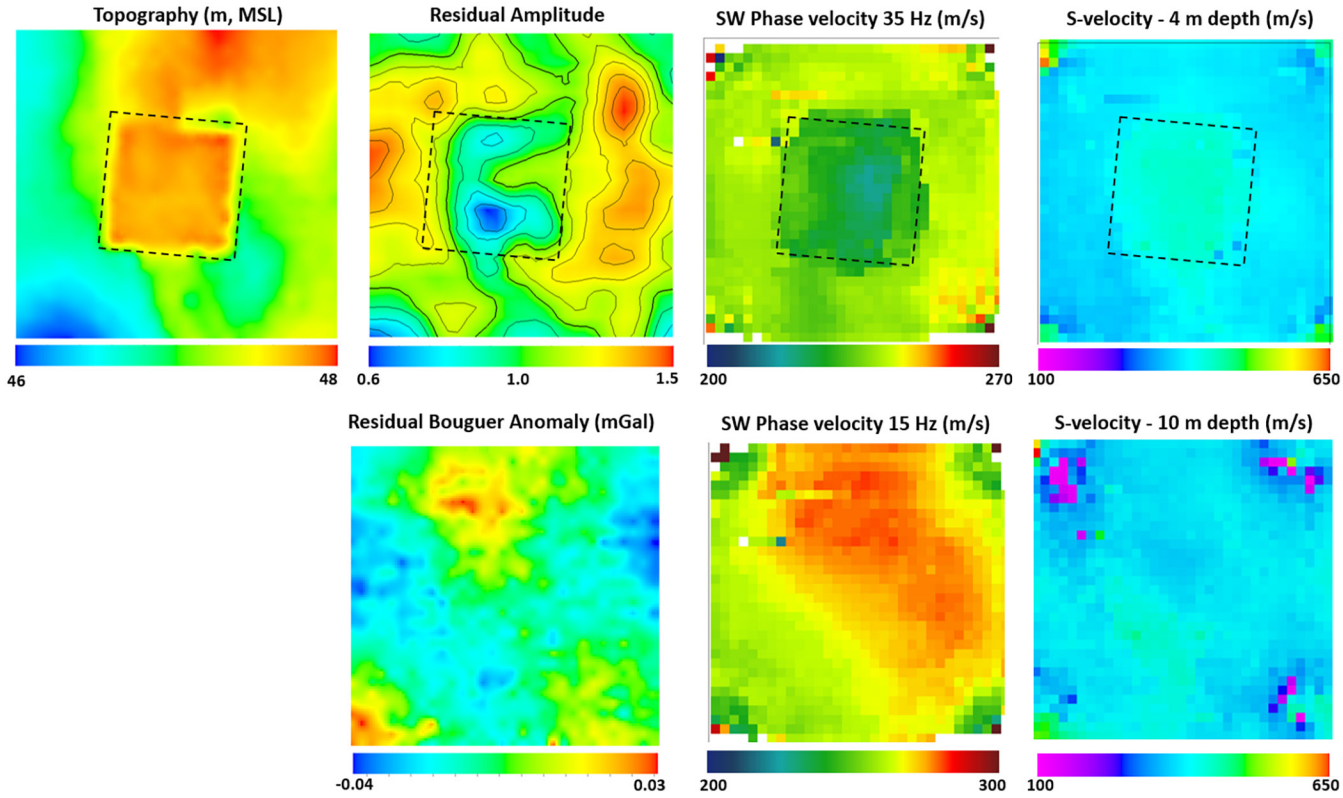

Figure 6. Pilot area 2 results. (top row) Very shallow geophysical attributes and V_S inversion, showing the sensitivity to an existing platform structure in the center of the investigated area. (bottom row) Deeper geophysical responses, indicating a predominantly 1D layered structure with no evidence of localized anomalies. The investigated area is 150 × 150 m with 5 × 5 m source and receiver spacing.

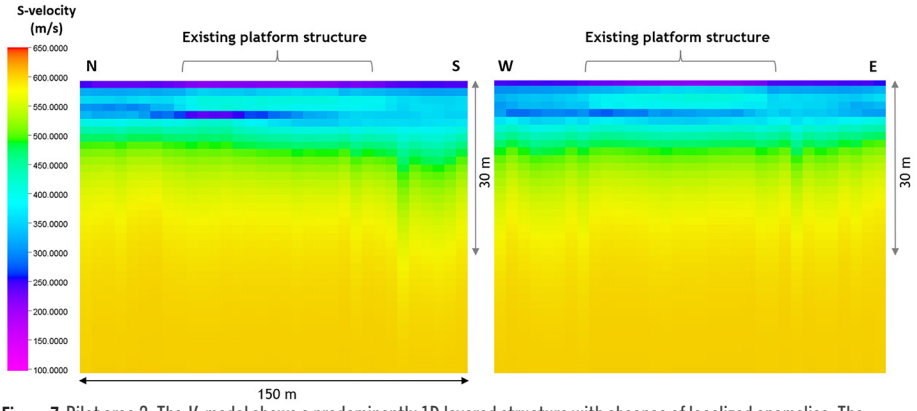

Figure 7. Pilot area 2. The V_S model shows a predominantly 1D layered structure with absence of localized anomalies. The shallow platform structure is properly mapped by the V_S inversion in both the spatial and vertical dimensions.

parameters show a predominant 1D structure with a possible slight tilt from north to south and from east to west (e.g., strike northwest-southeast, dip northeast-southwest). The platform structure is mapped also in the depth domain (Figure 7), where it is shown to be decoupled from the deeper predominantly 1D structure. No shallow geophysical anomalies that could be associated with voids/sinkholes are observed in pilot area 2.

Pilot area 3 also contains a platform structure, which is visible from the topographic map in Figure 8. This is flanked by depressions, representing areas where the soil was excavated to build the platform. We can also observe an access road in the northwest corner, with northeast–southwest orientation and an access road to the platform perpendicular to it. South of the platform structure, another elongated feature may be seen toward the southeast corner of the area. As per pilot area 2, we distinguish between the very shallow response (a few meters in depth) and a deeper response representing the undisturbed subsurface geology. Starting from the top row of Figure 8, we observe a slight response of the described features in the surface-consistent phase residual map and excellent ultra-resolution mapping from the surface-consistent residual amplitude map. Going deeper (bottom row of Figure 8), a predominantly 1D structure, possibly slightly tilted, can be observed from both the residual Bouguer microgravity map and the V_S depth slice at a depth of 16 m. The shallow subsurface structure at pilot area 3 does not present geophysical anomalies consistent with a developing geohazard. The recognizable details observed in the shallow layers and the decoupling of the shallow to deeper structures provide confidence in the conclusions.

Collapse site. A sinkhole developed, and the collapsed area was backfilled. Later, the area was investigated with shallow geophysics to verify the lateral and vertical extent of the subsurface cavity. Seismic data were acquired first by a network of densely spaced north–south and east–west crossing 2D lines and successively with a full nodal acquisition, with standard parameters of 5 × 5 m spaced nodes using a weight drop source. Results were

interpreted with the described method. Microgravity data were also acquired to support the interpretation. Results of the microgravity residual Bouguer anomaly and S-wave velocity modeling are shown in Figure 9. The follow-up verification boreholes confirmed the sinkhole structure as a localized vertical feature extending even beyond the maximum depth of exploration provided by surface-wave analysis (Figure 10). The stratigraphic columns derived from the shallow boreholes confirm the sharp vertical and lateral imaging obtained by shear velocity modeling.

Distributed karst. One final application is provided where geophysical investigation was performed for a shallow subsidence developed after heavy rains. Nodal acquisition was performed based on the geometry described in Figure 1, consisting of 5 × 5 m seismic node spacing and 2.5 × 5 m source spacing, where an autofire nitrogen-powered spring-accelerated hammer was used. Microgravity was also acquired over the 5 × 5 m grid to support the interpretation. The fast turnaround interpretation consisted of the described method, including the automatic picking of the surface-wave dispersion curves after surface-consistent preconditioning and S/N enhancement through VSG beam forming. Results indicate that the central/north section of the platform is affected by a broad low shear-velocity anomaly that is broadly confirmed by the residual Bouguer anomaly (Figure 11). The observed dynamic range is more than ±30 µGal (±0.03 mGal), which represents a range well above the targeted standard deviation of 5 µGal for the gravity measurements. Cross sections of the west, center, and east portions of the platform (Figure 12) suggest that the subsided location (arrow) is located at the edge of a wider area with distributed low velocity and low density.

The V_S cross sections (Figure 12) also show that the first 5 m of the ground is undisturbed across the whole surveyed area. This is consistent with the platform construction involving ground movement, leveling, and compaction. The section between 5 and 20 m is where the anomalies are observed, with large lateral variations occurring in a few tens of meters. The shallow localization of the subsidence is consistent with the visual observations of the collapse dynamics performed by the site operators. Subsidence of the area, surfacing of water forming a pool, final absorption/drainage of the water, and a depression because of the subsidence were observed. Such dynamics are consistent with a model of a shallow cavity (or network of cavities) filled with water, collapse of the roof, evacuation of the water to the surface, and final slow drainage.

Discussion and way forward

This section explores future developments, partly underway, that address the full utilization of a densely sampled seismic

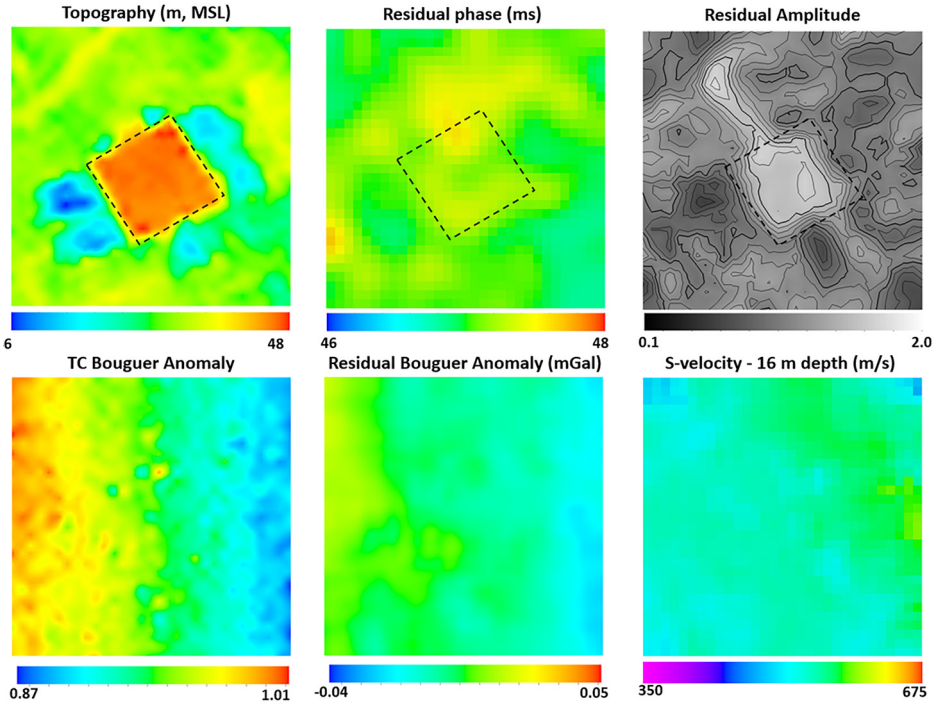

Figure 8. Pilot area 3. (top row) The very shallow geophysical attributes, and especially the residual amplitudes, provide mapping of the platform structure, as well as possible access roads. (bottom row) The slightly deeper geophysical response indicates a laterally continuous 1D structure. The investigated area is 150 × 150 m with 5 × 5 m source and receiver spacing.

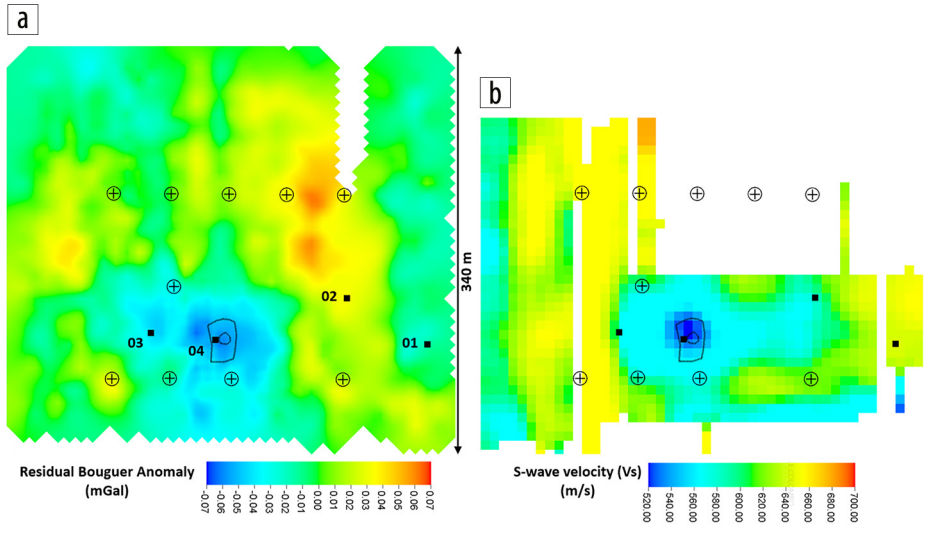

Figure 9. Collapse site results. (a) Gravity residual Bouguer anomaly. (b) S-wave velocity from surface-wave inversion. Location of verification boreholes are shown as black squares. Black lines indicate the extent of the surface collapse (inner circle) and the surface extent of the surface cracks and fissures (outer circle).

wavefield. The developed workflow addresses the requirement of a rapid and effective screening assessment for shallow geohazards, and it is tuned for the specific geologic conditions encountered. Additional analysis is ongoing, where an important addition is represented by high-frequency FWI, utilizing the VSG beam forming approach to enhance the S/N, followed by a 1.5D FWI scheme in the Laplace-Fourier domain (Colombo et al., 2021a). The challenges faced in FWI are related to the high frequency of the signal and the need to suppress the effect of large-amplitude surface waves, partly obtained by the application of Laplace-Fourier damping parameters from first-break traveltimes. The FWI step is considered important for enabling deeper modeling of the near surface in search of the root causes of the karst phenomena. Despite the attractive objective, the FWI step in the 1.5D approximation or with the full 3D implementation is inherently difficult to implement as a standard workflow for shallow geohazard investigation. Utilization of physics-driven ML inversion in velocity model building may provide significant advantages in enhancing the resolution, automating the process, and reducing the dependency of FWI on initial models, as shown by Colombo et al. (2024). Imaging either via seismic reflection surveys using P waves, horizontally polarized shear waves (Pugin et al., 2019), and/or through diffraction imaging (Moser and Howard, 2008) are other attractive directions requiring high-resolution acquisition parameters and a very large number of channels if 3D large source-receiver offsets (i.e., relative to the depth of the target) and submeter-scale receiver spacing are required. An attractive direction in the imaging domain is represented

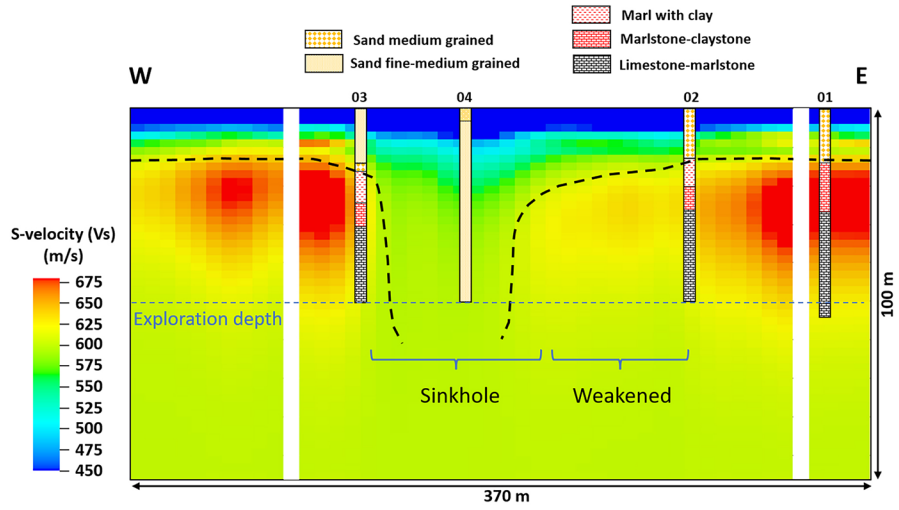

Figure 10. Sinkhole collapse. V_s cross section through the sinkhole area with verification boreholes.

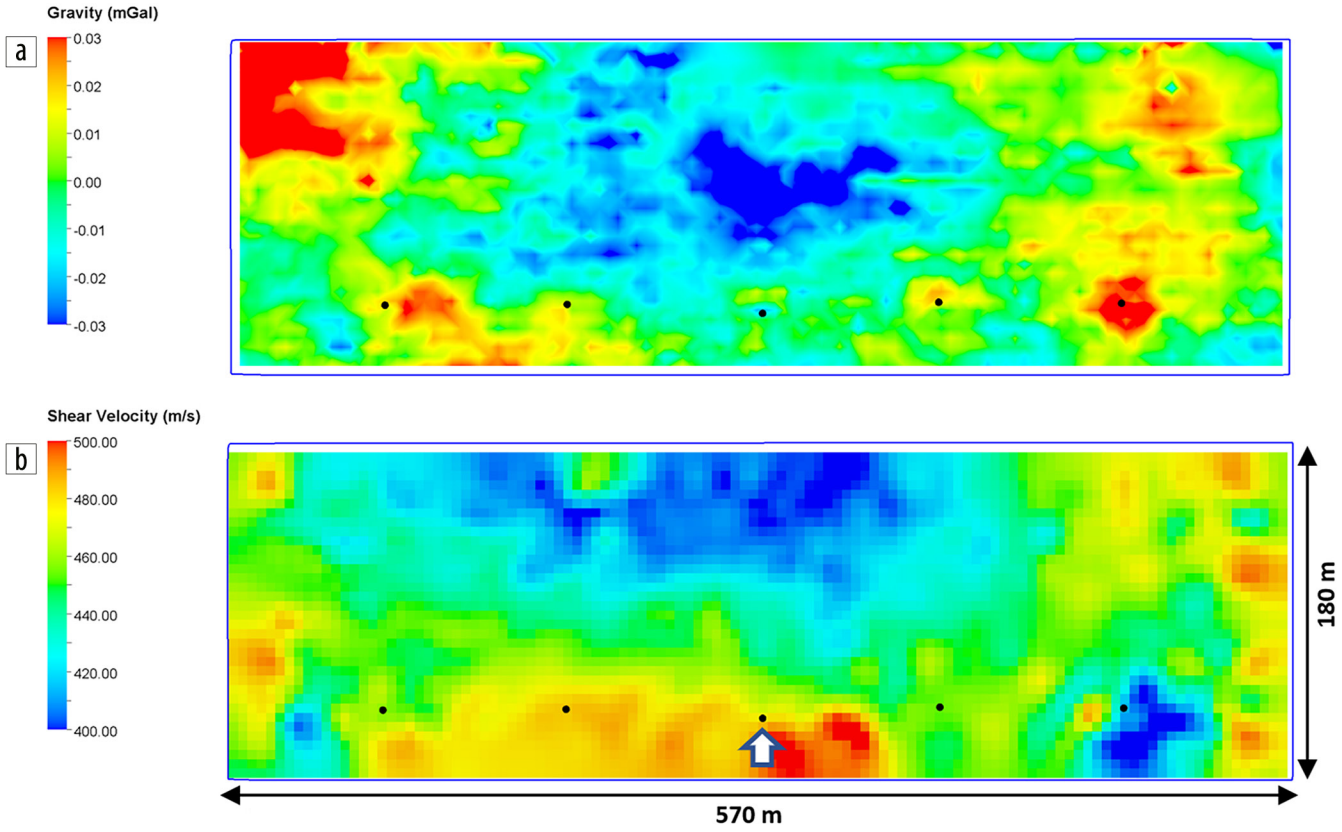

Figure 11. Distributed karst. Shallow geophysics results. (a) Residual Bouguer anomaly after standard corrections including terrain. (b) V_s at 10 m depth from the inversion of surface-wave dispersion curves.

by imaging scatterers, utilizing the backscattered analysis of surface waves and modifications of the original technique (Schwenk et al., 2016; Ivanov et al., 2017).

Scattered surface waves generated by near-surface heterogeneities can be spatially imaged (Campman et al., 2004). Reverse time migration of the recorded elastic wavefield can be used to image with good illumination the near-surface scatterers (Almuhaidib and Toksöz, 2015). These are topics of great interest that we plan to investigate soon. Analysis of passive recordings either via interferometry (Donno et al., 2021) or signal spectroscopy represents another important source of information for shallow geohazards to be considered in future developments. Seismic wavefield gradiometry (de Ridder and Curtis, 2017) is another important direction to be followed for analysis of the shallow geohazard problem, which also benefits from the dense spatial wavefield sampling provided by seismic nodes. Lastly, the research for effective shallow geohazard investigation should include multiphysics methods, where, in our experience, microgravity represents one of the most robust approaches that combines directly with seismic-based analysis. Other electrical- and electromagnetic-based approaches have not always been successful in the areas under investigation, likely due to an overall conductive substratum characterized by fine sediments and saline/brackish water close to the surface.

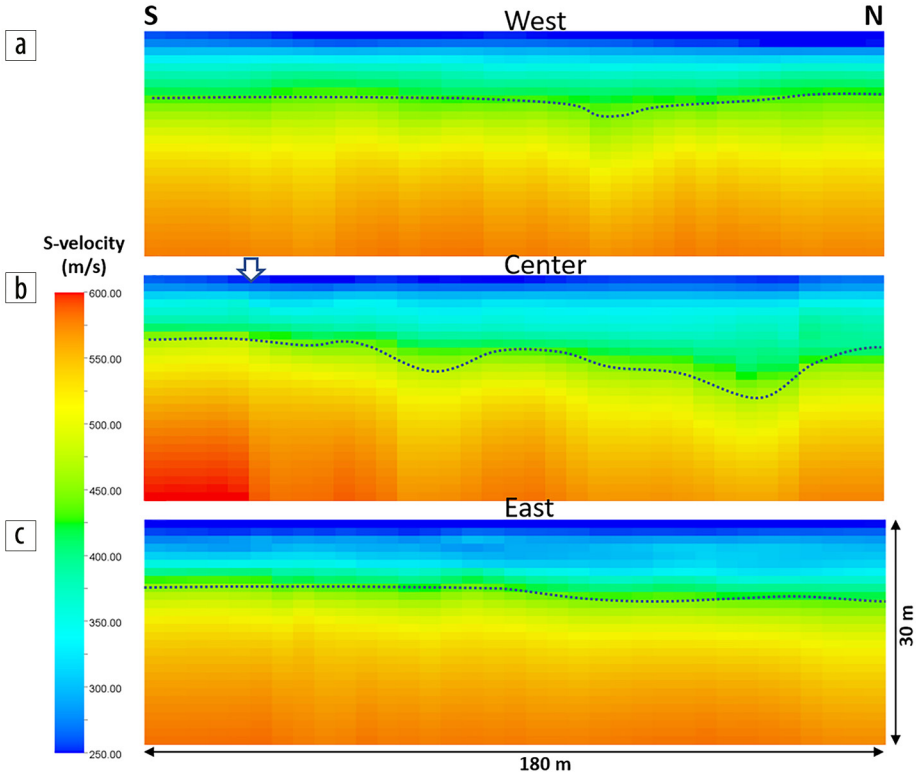

Figure 12. Distributed karst. Cross sections of the V_s field with the central section exhibiting large lateral velocity variations in the depth range from 5 to 20 m. The arrow indicates the location of the observed subsidence.

Conclusions

The developed workflow encompassing dense nodal seismic acquisition, transmitted wave surface-consistent decomposition and correction, beam forming via VSG, and ML-assisted processing and inversion is proving to be effective for the rapid scanning of near-surface-related geohazards. Data acquisition is fast, and analysis is largely automated. The large 3D nodal data set, detailed in the last example, was analyzed in three weeks. An independently performed conventional data analysis required six months of intensive work for deriving only a subset of the subsurface information. The developed acquisition and processing workflow provides multiattribute images and volumes of physical parameters describing the shallow subsurface conditions for effective decision making. The intelligent near-surface characterization objectives can expand toward the direction of FWI and imaging of multiple wave components, while leveraging the information provided by multiphysics methods. In this domain, dense microgravity measurements have proven to be the most effective in complementing the seismic-based results. TLE

Acknowledgments

We would like to acknowledge the detailed revision and helpful suggestions provided by Nori Nakata. Editors Julia Correa and Vladimir Kazei are also thanked for enhancing the quality and accuracy of the work.

Data and materials availability

Data associated with this research are confidential and cannot be released.

Corresponding author: daniele.colombodc@outlook.com

References

Almuhaidib, A. M., and M. N. Toksöz, 2015, Imaging of near-surface heterogeneities by scattered elastic waves: Geophysics, **80**, no. 4, A83–A88, https://doi.org/10.1190/geo2014-0416.1.

Alyousuf, T., D. Colombo, D. Rovetta, and E. Sandoval-Curiel, 2018, Near-surface velocity analysis for single-sensor data: An integrated workflow using surface waves, AI, and structure-regularized inversion: 88th Annual International Meeting, SEG, Expanded Abstracts, 2342–2346, https://doi.org/10.1190/segam2018-2994696.1.

Campman, X., K. van Wijk, C. Riyanti, J. Scales, and G. Herman, 2004, Imaging scattered seismic surface waves: Near Surface Geophysics, **2**, no. 4, 223–230, https://doi.org/10.3997/1873-0604.2004019.

Colombo, D., E. Turkoglu, E. Sandoval-Curiel, and T. Alyousuf, 2024, Self-supervised, active learning seismic full-waveform inversion: Geophysics, **89**, no. 2, U31–U52, https://doi.org/10.1190/geo2023-0308.1.

Colombo, D., E. Sandoval-Curiel, D. Rovetta, and A. Kontakis, 2021a, Near-surface full-waveform inversion in a transmission

DOI:10.1190/tle43080484.1

surface-consistent scheme: Geophysics, **86**, no. 2, U15–U29, https://doi.org/10.1190/geo2020-0474.1.
Colombo, D., E. Turkoglu, W. Li, E. Sandoval-Curiel, and D. Rovetta, 2021b, Physics-driven deep-learning inversion with application to transient electromagnetics: Geophysics, **86**, no. 3, E209–E224, https://doi.org/10.1190/geo2020-0760.1.
Colombo, D., D. Rovetta, E. Sandoval-Curiel, and A. Kontakis, 2020, Transmission-based near-surface deconvolution: Geophysics, **85**, no. 2, V169–V181, https://doi.org/10.1190/geo2019-0443.1.
Colombo, D., F. Miorelli, E. Sandoval, and K. Erickson, 2016, Fully automated near-surface analysis by surface-consistent refraction method: Geophysics, **81**, no. 4, U39–U49, https://doi.org/10.1190/geo2016-0018.1.
De Ridder, S., and A. Curtis, 2017, Seismic gradiometry using ambient seismic noise in an anisotropic earth: Geophysical Journal International, **209**, no. 2, 1168–1179, https://doi.org/10.1093/gji/ggx073.
Dean, T., J. Tulett, and R. Barnwell, 2018, Nodal land seismic acquisition: The next generation: First Break, **36**, no. 1, 47–52, https://doi.org/10.3997/1365-2397.n0061.
Donno, D., M. S. Farooqui, M. Khalil, D. McCarthy, D. Solyga, J. Courbin, A. Prescott, L. Delmas, and D. Le Meur, 2021, Multiwave inversion: A key step for depth model building — Examples from the Sultanate of Oman: The Leading Edge, **40**, no. 8, 610–618, https://doi.org/10.1190/tle40080610.1.
Ester, M., H.-P. Kriegel, J. Sander, and X. Xu, 1996, A density-based algorithm for discovering clusters in large spatial databases with noise: Presented at the 2nd International Conference on Knowledge Discovery and Data Mining.
Ivanov, J., R. D. Miller, D. Z. Feigenbaum, and S. L. Peterie, 2017, Detecting subsurface objects and identifying voids possibilities using the backscatter analysis of surface wave (BASW) method: Presented at the International Conference on Engineering Geophysics.
Li, J., and S. Hanafy, 2016, Skeletonized inversion of surface wave: Active source versus controlled noise comparison: Interpretation, **4**, no. 3, SH11–SH19, https://doi.org/10.1190/int-2015-0174.1.
Miao, X., D. Zheng, L. Zi, Z. Zhou, and M. Gao, 2016, Robust multimodal surface-wave inversion for shallow velocity and shear statics: 86th Annual International Meeting, SEG, Expanded Abstracts, 4956–4960, https://doi.org/10.1190/segam2016-13822744.1.
Moser, T., and C. Howard, 2008, Diffraction imaging in depth: Geophysical Prospecting, **56**, no. 5, 627–641, https://doi.org/10.1111/j.1365-2478.2007.00718.x.
Ourabah, A., 2024, Revisiting the single sensor vs array debate in the light of new nodal system technology: First Break, **42**, no. 1, 71–77, https://doi.org/10.3997/1365-2397.fb2024006.
Park, C. B., R. D. Miller, and J. Xia, 1999, Multichannel analysis of surface waves: Geophysics, **64**, no. 3, 800–808, https://doi.org/10.1190/1.1444590.
Pugin, A. J.-M., K. Brewer, T. Cartwright, and S. L. Sargent, 2019, Detection of tunnels and boulders using shallow SH-SH reflected seismic waves: The Leading Edge, **38**, no. 6, 436–441, https://doi.org/10.1190/tle38060436.1.
Rovetta, D., A. Kontakis, and D. Colombo, 2021, Application of a density-based spatial clustering algorithm for fully automatic picking of surface-wave dispersion curves: The Leading Edge, **40**, no. 9, 678–685, https://doi.org/10.1190/tle40090678.1.
Roy, S., E. Kocel, N. Dyaur, and R. R. Stewart, 2013, Lateral heterogeneity and surface-wave inversion (MASW): 83rd Annual International Meeting, SEG, Expanded Abstracts, 1909–1913, https://doi.org/10.1190/segam2013-1084.1.
Schwenk, J. T., S. D. Sloan, J. Ivanov, and R. D. Miller, 2016, Surface-wave methods for anomaly detection: Geophysics, **81**, no. 4, EN29–EN42, https://doi.org/10.1190/geo2015-0356.1.
Socco, L. V., S. Foti, and D. Boiero, 2010, Surface-wave analysis for building near-surface velocity models — Established approaches and new perspectives: Geophysics, **75**, no. 5, 75A83–75A102, https://doi.org/10.1190/1.3479491.
Socco, L. V., D. Boiero, S. Foti, and R. Wisén, 2009, Laterally constrained inversion of ground roll from seismic reflection records: Geophysics, **74**, no. 6, G35–G45, https://doi.org/10.1190/1.3223636.
Taner, M. T., and F. Koehler, 1981, Surface consistent corrections: Geophysics, **46**, no. 1, 17–22, https://doi.org/10.1190/1.1441133.
Taner, M. T., F. Koehler, and K. Alhilali, 1974, Estimation and correction of near-surface time anomalies: Geophysics, **39**, no. 4, 441–463, https://doi.org/10.1190/1.1440441.
Xia, J., R. D. Miller, C. B. Park, and G. Tian, 2003, Inversion of high frequency surface waves with fundamental and higher modes: Journal of Applied Geophysics, **52**, no. 1, 45–57.
Zecka, M., K. Van Noten, and T. Lecocq, 2022, Sensitivity, accuracy and limits of the lightweight three-component SmartSolo geophone sensor (5 Hz) for seismological applications: eartharxiv, https://doi.org/10.31223/X5F073.